Earthquake Engineering & Structural Dynamics
The Journal of the International Association for Earthquake Engineering

EARTHQUAKE ENGINEERING & STRUCTURAL DYNAMICS
Earthquake Engng Struct. Dyn. (2013)
Published online in Wiley Online Library (wileyonlinelibrary.com). DOI: 10.1002/eqe.2311

Dynamics of inelastic base-isolated structures subjected to analytical pulse ground motions

Michalis F. Vassiliou*,†, Anastasios Tsiavos and Božidar Stojadinović

Institute of Structural Engineering, Swiss Federal Institute of Technology (ETH) Zürich, 8093, Zurich, Switzerland

SUMMARY

Structural design code provisions worldwide prescribe relatively small seismic force reduction factors for seismically base-isolated structures, making their response to design-level earthquake excitation essentially elastic. This paper uses the method of dimensional analysis to prove that; in most cases, this is not a conservative design approach but a necessity that emerges from the dynamics of base-isolated structures. It is shown that allowing typical base-isolated structures to yield results in large displacement ductility demands for the structure. This phenomenon is caused by the change in the nature of the ground motion excitation as it is transmitted to the structure through the seismic base isolation system as well as by the change in the distribution of displacements between the structure and the isolation bearings caused by yielding of the isolated structure. Copyright © 2013 John Wiley & Sons, Ltd.

Received 4 September 2012; Revised 10 April 2013; Accepted 21 April 2013

KEY WORDS: seismic isolation; inelastic response; pulse excitation; force reduction factors

1. INTRODUCTION

There is a consensus in the earthquake engineering community that designing buildings to remain elastic under large seismic loads corresponding to the design-basis hazard level is financially irrational. Modern seismic design codes permit structures that are expected to deform well into their inelastic response range during design-basis earthquakes. Preventing collapse of such structures is made possible simultaneously by the oscillatory nature and randomness of earthquake excitation and by capacity design and detailing of structural elements and systems. Accordingly, seismic design codes prescribe acceptable plastic deformation limits in terms of structure displacement ductility μ for different structural systems at the design-basis earthquake hazard level. Then, in accordance with the equivalent seismic force design approach, the codes provide designers with force reduction factors R (ASCE 7 [1]) or behavior factors q (Eurocode [2]), both defined as the ratio of the base shear required for the building to remain elastic to the design base shear. Numerous studies on the relationship between R (or q) and μ have been published [3–11]. All agree that for flexible structures, R is equal to μ ('equal displacement' rule) and that for stiff structures, R is less than μ (maximum displacement of the inelastic structure is larger than that of the elastic structure with the same fundamental mode vibration period). For very stiff structures, displacement ductility μ becomes very large even for small values of R, that is, seismic force demand only slightly in excess of the yield force capacity of the structure induces a very large displacement ductility demand. Values of the strength reduction factor range between 2 and 8. Experience from recent earthquakes shows that the inelastic design approach works well to save lives by preventing the collapse of most

*Correspondence to: Michalis F. Vassiliou, Institute of Structural Engineering, Swiss Federal Institute of Technology (ETH) Zürich, 8093 Zurich, Switzerland.
†E-mail: mfvassiliou@gmail.com

structures. However, the societal losses due to structural damage and, more importantly, damage that causes disruption or loss of the intended function of the structures in the earthquake-affected region are enormous.

Seismic base isolation is a well-known technique to modify the seismic response of a structure to protect it against collapse, minimize its permanent deformation, and control the relative drifts and accelerations that contribute to non-structural damage [12], thereby significantly improving the chances that the intended function of the structure will be preserved after an earthquake. Typically, a structure is placed on a system of bearings, rubber, or sliding, with low horizontal stiffness. Thus, the fundamental vibration period of the structure–isolator system becomes several (2 to 4) times longer than the vibration period of the structure fixed to the ground. Typically, isolation leads to a corresponding twofold to fourfold decrease in the seismic base shear force for the isolation system and, by equilibrium, for the structure at the expense of large deformation demand for the seismic isolation bearings.

Current European, Japanese, and US seismic design codes limit the magnitude of strength reduction allowed for base-isolated structures. The Eurocode [2] allows a maximum behavior factor value of 1.5 for seismically isolated buildings, similar to the nonlinear analysis with peer review option of the Japanese building code [13]. US ASCE 7 [1] allows the strength reduction factor for a seismically isolated structure to be 0.375 times the one for a corresponding fixed-base structure and no larger than 2. Such designs result in good behavior of seismically isolated building structures observed in recent earthquakes (e.g., [14]). Design codes do not explicitly state the reason for keeping the response of base-isolated structures in the essentially elastic range. Research results published by Constantinou and Quarshie [15], Ordonez *et al*. [16], Kikuchi *et al*. [17], and Thiravechyan *et al*. [18] indicate that inelastic deformation of base-isolated structures, if it occurs, may be much larger than expected.

The consequence of these design code provisions is the design base shear for base-isolated structures that is often equal to or larger than that for the same fixed-base structure [19]. This means that the cost to build a base-isolated structure is often higher than that for a corresponding fixed-base structure, leading many investors to choose low initial investment costs and accept the higher risk of business interruption and repair losses over the lifetime of the structure.

In this paper, we use the method of dimensional analysis to investigate the dynamics of inelastic base-isolated structures responding to analytical pulse excitation. We find that relatively stiff base-isolated structures whose strength is less than that required to remain elastic develop significantly larger displacement ductility demands than similarly stiff and strong fixed-base structures under the same excitation. This behavior, demonstrated for pulse-like excitation in this paper, extends on the results of Kikuchi *et al*. [17] and Thiravechyan *et al*. [18] obtained for sinusoidal excitation. This finding indicates that the US, Japanese, and European design code strength requirements for base-isolated structures are justified.

2. REVIEW OF R_y–μ–T_S RELATIONSHIPS FOR FIXED-BASE STRUCTURES

We aim to compare the seismic response of an inelastic single-degree-of-freedom (SDOF) system with a vibration period T_s to that of an equivalent linear-elastic system (an SDOF system with the same vibration properties that is strong enough not to yield under the same excitation). The response of the inelastic SDOF system is hysteretic and follows a bilinear elastic–plastic response envelope. The maximum displacements of the elastic and of the inelastic systems are denoted as u_{el} and u_m, respectively. The yield displacement of the inelastic system is denoted as u_y. The maximum force of the elastic system is denoted as F_{el} and the yield force of the inelastic system as F_y. The force reduction factor, R_y, is defined in this study as

$$R_y = \frac{F_{el}}{F_y} \tag{1}$$

DOI: 10.1002/eqe

and the displacement ductility, μ, of the system is defined as

$$\mu = \frac{u_m}{u_y} \tag{2}$$

Note that the principal difference between R_y used in this study and R used in design codes is that R accounts for structural overstrength. For a given excitation, the relation between R_y and μ can be parameterized by T_s [20]. Numerous researchers developed relations between R_y, μ, and T_s on the basis of statistical processing of the seismic response data for elastic and inelastic SDOF structure responses to recorded earthquake ground motions. Miranda and Bertero [10] comprehensively present and compare the R_y–μ–T_s relationships available in literature. Two findings are common across the reviewed literature. First, there exists a period T_c such that SDOF structures with a vibration period $T_s > T_c$ attain roughly the same maximum displacement regardless of their response mode, linear elastic or inelastic ($u_m \approx u_{el}$). In other words, 'equal displacement' rule holds; hence, $R_y \approx \mu$. Second, displacements of inelastic SDOF structure with $T_s < T_c$ are larger than those of the corresponding linear-elastic SDOF structures, that is, $u_m > u_{el}$, leading to $R_y < \mu$. Finally, R_y decreases and tends to 1 as T_s tends to zero for very stiff structures. It is important to underline that even though the displacements of the inelastic and the linear-elastic very stiff structures are small, the displacement ductility demand for such structures may be very large because their yield displacements are also small. Therefore, the conventional form of R_y–μ–T_s relation may not represent the actual displacements of very stiff structures accurately because ductility is computed as a ratio of two small values. Nevertheless, the conventional R_y–μ–T_s relationship format is used in this study to facilitate a comparison to a significant body of knowledge found in the literature.

Miranda [21], and Ruiz-Garcia and Miranda [22] showed that the R_y–μ–T_s relation changes depending on the soil at the site of the structure and noted that the displacement ductility demands for stiff structures grow as the soil becomes softer. An analogy between soft soils and seismic isolation systems in terms that both have low horizontal stiffness and permit significant lateral displacements inspired the work presented in this paper.

3. LINEAR-ELASTIC MODEL OF A BASE-ISOLATED STRUCTURE

Kelly [12] developed a linearized 2-degree-of-freedom model to describe the behavior of base-isolated structures (Figure 1). Even though the inelastic response of most seismic isolation bearings can be effectively modeled using a bilinear hysteretic law, a linearized bearing model based on the post-yield

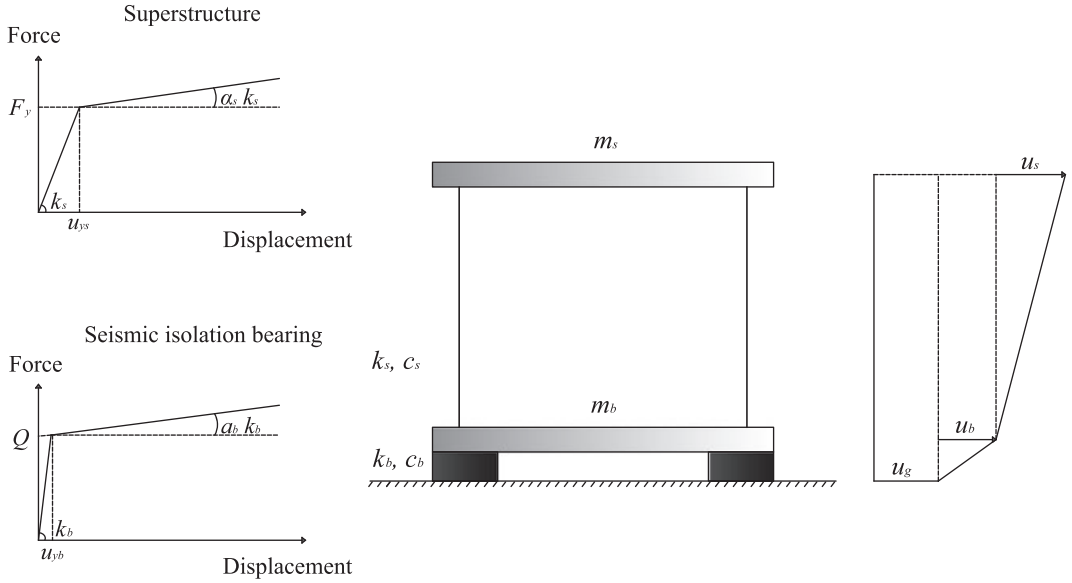

Figure 1. Parameters of the 2-DOF model of a base-isolated structure.

DOI: 10.1002/eqe

stiffness of the bearings gives insight into the dynamics of base-isolated structures. In Figure 1, m_b represents the mass of the base mat above the seismic isolation system, m_s is the mass of the isolated structure, u_s is the deformation of the superstructure with respect to the base mat, and u_b is the deformation of the bearings with respect to the ground. The following quantities are defined:

(1) Fixed-base period and cyclic frequency

$$T_s = 2\pi\sqrt{\frac{m_s}{k_s}}, \omega_s = \sqrt{\frac{k_s}{m_s}} \tag{3}$$

(2) Isolation period and cyclic frequency

$$T_b = 2\pi\sqrt{\frac{m_s + m_b}{\alpha_b k_b}}, \omega_b = \sqrt{\frac{\alpha_b k_b}{m_s + m_b}} \tag{4}$$

(3) Period ratio

$$\varepsilon = \frac{{T_s}^2}{{T_b}^2} \tag{5}$$

(4) Structural and isolation damping ratio

$$\xi_s = \frac{c_s}{2m_s\omega_s}, \qquad \xi_b = \frac{c_b}{2(m_s + m_b)\omega_b} \tag{6}$$

(5) Mass ratio

$$\gamma_m = \frac{m_s}{m_s + m_b} \tag{7}$$

Modal analysis of this linearized seismic isolation system gives modal frequencies:

$${\omega_1}^2 = {\omega_b}^2(1 - \gamma\varepsilon) \quad {\omega_2}^2 = \frac{{\omega_s}^2}{1 - \gamma}(1 + \gamma\varepsilon) \tag{8}$$

and vibration mode shapes:

$${\Phi^1}^{\mathrm{T}} = (1, \varepsilon) \qquad {\Phi^2}^{\mathrm{T}} = \left(1, -\frac{1}{\gamma}(1 - (1 - \gamma)\varepsilon)\right) \tag{9}$$

The horizontal displacements of the seismic isolation bearings and the structure are (after neglecting the higher-order ε terms)

$$u_{\mathrm{b\,max}} = (1 - \gamma\varepsilon)S_{\mathrm{D}}(\omega_1, \xi_1) \tag{10}$$

$$u_{\mathrm{s\,max}} = \varepsilon\left(S_D(\omega_1, \xi_1)^2 + S_{\mathrm{D}}(\omega_2, \xi_2)^2\right)^{1/2} \tag{11}$$

where ξ_1 and ξ_2 are the modal damping ratios. When the structure is much stiffer than the seismic isolation system, it follows that the period ratio ε is small ($\varepsilon = O(10^{-2})$), and the spectral displacements for the two vibration modes of the system are very different ($S_{\mathrm{D}}(\omega_2,\xi_2) << S_{\mathrm{D}}(\omega_1,\xi_1)$). Hence, most of the horizontal displacements is concentrated in the isolation bearings while the structure deforms only slightly. However, when the structure and the seismic isolation system

DOI: 10.1002/eqe

have similar stiffness, the period ratio ε is not small, and the spectral displacement values are comparable, leading to a conclusion that the displacements of the seismic isolation system and the structure are comparable in magnitude.

4. INELASTIC MODEL OF A BASE-ISOLATED STRUCTURE

The model used in this study is the 2-DOF model proposed by Kelly [12] (Figure 1) modified to account for inelastic response of both the isolation bearings and of the isolated structure. The bearing response is modeled using a bilinear response envelope with hysteretic damping, a good model for both rubber and spherical sliding bearings. The bilinear hysteretic behavior is implemented using a Bouc–Wen [23, 24] model. Sometimes, designers provide additional viscous damping for the isolation system. Hence, the restoring force of the isolation system is modeled as

$$F_{\mathrm{b}}(t) = -\alpha_{\mathrm{b}} k_{\mathrm{b}} u_{\mathrm{b}}(t) - Q \cdot z_{\mathrm{b}}(t) - c_{\mathrm{b}} \dot{u}_{\mathrm{b}}(t) \tag{12}$$

where $\alpha_{\mathrm{b}} k_{\mathrm{b}}$ is the second slope of the bilinear response envelope (Figure 1), c_{b} is the damping coefficient of the viscous dampers, Q is the strength of the system (force at zero displacement), and $z(t)$ is a dimensionless parameter of the Bouc–Wen model given by the evolution equation:

$$\dot{z}_{\mathrm{b}}(t) = \frac{1}{u_{\mathrm{y_b}}} \left(\dot{u}_{\mathrm{b}}(t) - \gamma_{\boldsymbol{BW}} |\dot{u}_{\mathrm{b}}(t)| z_{\mathrm{b}}(t) |z_{\mathrm{b}}(t)|^{n-1} - \beta \dot{u}_{\mathrm{b}}(t) |z_{\mathrm{b}}(t)|^{n} \right), \tag{13}$$

where u_{yb} is the yield displacement of the bilinear model and β, γ_{BW}, and n are dimensionless quantities that control the hysteretic behavior of the model. Parameters β and γ_{BW} are set equal to 0.5, and n is set equal to 8 to obtain a sharp transition from the first to the second slope of the response envelope.

The isolated structure is modeled using a bilinear Bouc–Wen model in parallel with a viscous damper. The restoring force of the isolated structure is given by

$$F(t) = -\alpha_{\mathrm{s}} k_{\mathrm{s}} u_{\mathrm{s}}(t) - (1 - \alpha_{\mathrm{s}}) k_{\mathrm{s}} u_{\boldsymbol{y}_{\mathrm{s}}} z_{\mathrm{s}}(t) - c_{\mathrm{s}} \dot{u}_{\mathrm{s}}(t) \tag{14}$$

where $u_{\mathrm{s}}(t)$ is the displacement of the structure relative to the base mat, k_{s} the pre-yield (elastic) stiffness, u_{ys} the yield displacement, α_{s} the hardening ratio of post-yield to pre-yield stiffness (Figure 1), c_{s} is the damping coefficient, and $z_{\mathrm{s}}(t)$ the dimensionless hysteretic parameter given by the evolution equation:

$$\dot{z}_{\mathrm{s}}(t) = \frac{1}{u_{\boldsymbol{y}_{\mathrm{s}}}} \left(\dot{u}_{\mathrm{s}}(t) - \gamma_{\boldsymbol{BW}} |\dot{u}_{\mathrm{s}}(t)| z_{\mathrm{s}}(t) |z_{\mathrm{s}}(t)|^{n-1} - \beta \dot{u}_{\mathrm{s}}(t) |z_{\mathrm{s}}(t)|^{n} \right) \tag{15}$$

The yield strength of the structure is

$$F_{\boldsymbol{y}} = k_{\boldsymbol{s}} u_{\boldsymbol{y}_{\boldsymbol{s}}} \tag{16}$$

Dynamic equilibrium of the structure and the base isolation system gives

$$(m_{\mathrm{s}} + m_{\mathrm{b}}) \ddot{u}_{\mathrm{b}} + m_{\mathrm{s}} \ddot{u}_{\mathrm{s}} + \alpha_{\mathrm{b}} k_{\mathrm{b}} u_{\mathrm{b}} + Q z_{\mathrm{b}}(t) + c_{\mathrm{b}} \dot{u}_{\mathrm{b}}(t) = -(m_{\mathrm{s}} + m_{\mathrm{b}}) \ddot{u}_{\mathrm{g}} \tag{17}$$

Dynamic equilibrium of the isolated structure gives

$$m_{\mathrm{s}} \ddot{u}_{\mathrm{s}} + m_{\mathrm{s}} \ddot{u}_{\mathrm{b}} + \alpha_{\mathrm{s}} k_{\mathrm{s}} u_{\mathrm{s}} + (1 - a_{\mathrm{s}}) k_{\mathrm{s}} u_{\mathrm{y_s}} z_{\mathrm{s}} + c_{\mathrm{s}} \dot{u}_{\mathrm{s}} = -m_{\mathrm{s}} \ddot{u}_{\mathrm{s}} \tag{18}$$

DOI: 10.1002/eqe

Consequently, equations (17) and (18) become equations of motion of the combined structure–isolation system. The results presented in this study were obtained by solving the conventionally derived equations (19) and (20) by using Matlab The Mathworks, Inc.: Natick, MA, 1999.

$$\ddot{u}_{\mathrm{b}} + \gamma_{\boldsymbol{m}}\ddot{u}_{\mathrm{s}} + {\omega_{\mathrm{b}}}^2 u_{\mathrm{b}} + \frac{Q}{m_{\mathrm{s}} + m_{\mathrm{b}}} z_{\mathrm{b}} + 2\xi_{\boldsymbol{b}}\omega_{\boldsymbol{b}}\dot{u}_{\boldsymbol{b}} = -\ddot{u}_{\mathrm{g}} \tag{19}$$

$$\ddot{u}_{\mathrm{s}} + \ddot{u}_{\mathrm{b}} + \alpha_{\mathrm{s}}{\omega_{\mathrm{s}}}^2 u_{\mathrm{s}} + (1-\alpha_{\mathrm{s}}){\omega_{\mathrm{s}}}^2 u_{\mathrm{y_s}} z_{\mathrm{s}} + 2\xi_{\mathrm{s}}\omega_{\mathrm{s}}\dot{u}_{\mathrm{s}} = -\ddot{u}_{\mathrm{g}} \tag{20}$$

5. RESPONSE OF A BASE-ISOLATED STRUCTURE TO ANALYTICAL PULSE EXCITATION

An analytical symmetric Ricker pulse (Ricker 1943[25], 1944[26]) with a pulse period $T_{\mathrm{p}} = 0.5$ and pulse peak acceleration $a_{\mathrm{p}} = 0.8\,g$ (Figure 2, left) given by

$$\ddot{u}_{\mathrm{g}}(t) = a_{\mathrm{p}}\left(1 - \frac{2\boldsymbol{\pi}^2 t^2}{T_{\mathrm{p}}^2}\right)\boldsymbol{e}^{-\frac{12\boldsymbol{\pi}^2 t^2}{2\ T_{\mathrm{p}}^2}} \tag{21}$$

is used to excite a prototype SDOF structure with mass $m_{\mathrm{s}} = 100$ t, structural vibration period $T_{\mathrm{s}} = 0.5$ s, and damping ratio $\zeta = 0.02$. Four different instances of the prototype structures are developed, all having the same mass, vibration period, and damping. First, the strengths of the fixed-base prototype structure are selected such that it responds elastically ($R_{\mathrm{y}} = 1$) and inelastically ($R_y = 2$, $\alpha = 0.02$) to the chosen Ricker pulse. Second, the prototype structure is base isolated using spherical sliding bearings. The mass of the structure and the base mat are assumed to be the same, resulting in a mass ratio $\gamma_{\mathrm{m}} = 0.5$. The bearing system stiffness k_{b} is selected such that the isolation period $T_{\mathrm{b}} = 3$ s. The bearing friction coefficient $\mu_{\mathrm{f}} = 0.05$ is selected such that the strength of the bearings system $Q = \mu_{\mathrm{f}}(m_{\mathrm{s}} + m_{\mathrm{b}})g = 98.1$ kN, approximately 20 times less than the strength of the elastic fixed-base structure (=1869 kN). Such relatively weak bearing system is selected to starkly highlight the difference in the response of elastic and inelastic isolated structures. The strengths of the fixed-base and base-isolated prototype structures are selected such that they remain elastic ($R_{\mathrm{y}} = 1$) or yield ($R_{\mathrm{y}} = 2$, $\alpha_{\mathrm{s}} = 0.02$) when excited by the chosen Ricker pulse. The structural characteristics of the four instances of the prototype structure are shown in Table I.

The force–deformation responses of the four structures to the chosen symmetric Ricker pulse are shown in Figure 3. The plot in Figure 3 (top-left) shows that the inelastic fixed-base prototype structure, with $R_{\mathrm{y}} = 2$, develops a displacement ductility $\mu = \frac{0.11m}{0.06m} = 1.83$ confirming the validity of

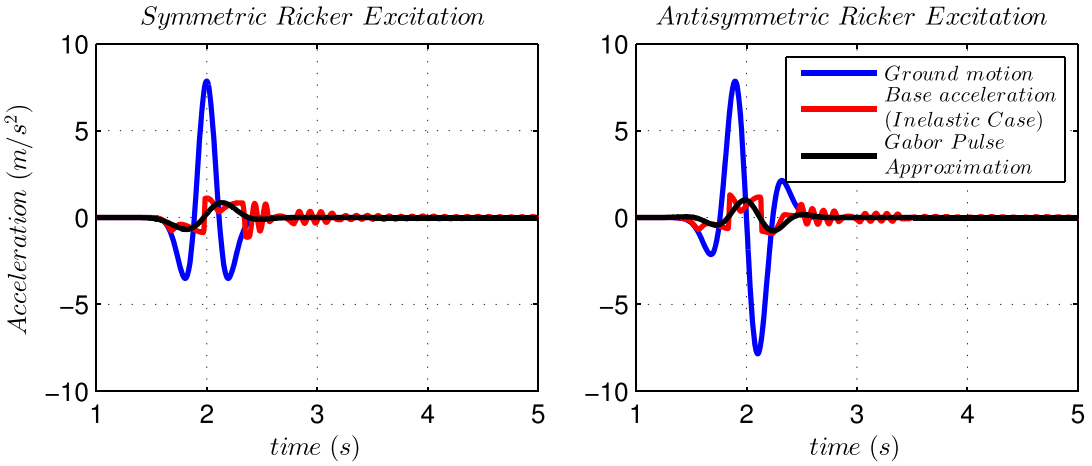

Figure 2. Acceleration time histories of the symmetric (left) and antisymmetric (right) Ricker pulse ground motion excitations, the response of the base mat, and a Gabor pulse approximation of the base mat response.

DOI: 10.1002/eqe

Table I. Yield displacement and strength of four instances of the prototype structure.

Prototype SDOF structure $m_s = 100$ t; $T_s = 0.5$ *s*	Fixed-base	Base-isolated $T_b = 3$ s; $Q = 98.1$ kN, $\gamma_m = 0.5$
Elastic ($R_y = 1$)	$u_y = 118$ mm; $F_y = 1869$ *kN*	$u_y = 8$ mm; $F_y = 123.6$ *kN*
Inelastic ($R_y = 2$)	$u_y = 59$ mm; $F_y = 934.5$ *kN*	$u_y = 4$ mm; $F_y = 61.8$ *kN*

the 'equal displacement' rule ($R_y \approx \mu$) for the relatively short vibration period $T_s = 0.5$ s. The strength of the elastic base-isolated structure is an order of magnitude smaller than that of the corresponding elastic fixed-base structure (Table I), confirming the effectiveness of the base isolation system in decreasing the base shear demand for the isolated structure. However, if the base-isolated structure is designed with $R_y = 2$ to respond inelastically (Figure 3(top-right)), it develops a displacement ductility demand $\mu = \frac{0.023m}{0.004m} = 5.75$, significantly more than expected using the 'equal displacement' rule.

A comparison of response plots in Figure 3 shows that the relative displacement of the elastic base-isolated structure (u_s) is an order of magnitude smaller than the displacement of the base mat (u_b) or the total displacement of the structure relative to the ground ($u_s + u_b$). However, the relative displacement of the inelastic base-isolated structure is not negligible (in this case, it is approximately a third of the bearing displacement). Note that the displacement of the base mat is approximately the same for the elastic and the inelastic base-isolated structures, confirming an observation made by Kikuchi *et al.* [17] that the maximum displacement of the base mat is minimally affected by the yielding of the structure. Makris and Kampas [27] have recently shown that the isolation period T_b is a good descriptor of the frequency content of the response

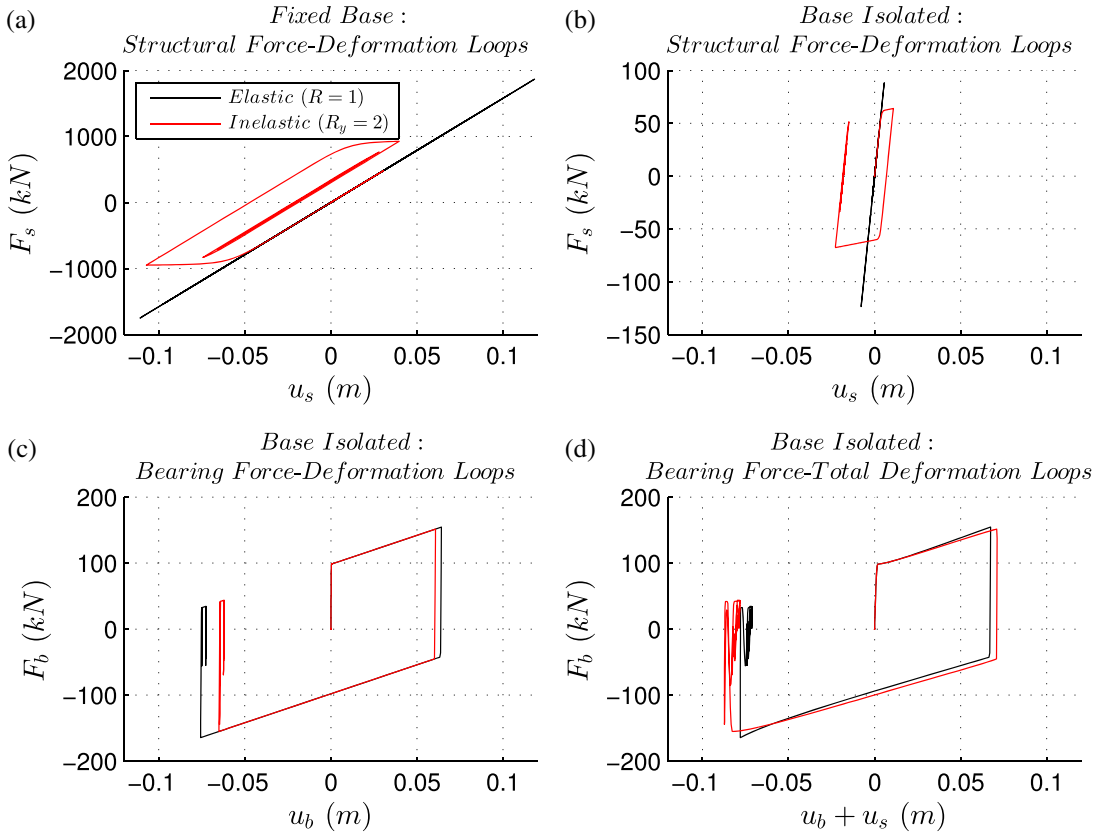

Figure 3. Force–deformation loops of (a) fixed-base elastic and inelastic structure, (b) seismically isolated elastic and inelastic structure, and (c) isolation bearings (for elastic and inelastic structure). (d) Bearing force–total (bearing + structural) displacement loops. The excitation is a symmetric Ricker pulse.

DOI: 10.1002/eqe

of the isolated structure (better than the secant period T_{eff} used in design codes [1, 2]). These two findings justify the use of the post-yield bearing stiffness in the dimensional analysis of the response of the isolated structures.

The departure of the response of the inelastic base-isolated structure from the equal displacement rule may be explained by observing that base isolation not only decreases the magnitude of the excitation transmitted to the isolated structure but also lengthens the dominant period of the motion of the base mat, thus changing the nature of the excitation of the isolated structure. Such lengthening of dominant period of the excitation is detrimental to classes of structures whose response is strongly dependent on the period of the excitation, such as the elastoplastic fixed-base structures (Makris and Black [28, 29]) and rocking structures (Vassiliou and Makris [30]). The base (ground) acceleration of the fixed-base structure is compared with the base mat acceleration of the isolated structure for the symmetric excitation (Figure 2—left). The motion of the isolated base mat is pulse-like: it was analyzed using wavelet analysis (Vassiliou and Makris [31]) to extract its dominant period. This dominant period is 0.88 s, significantly longer than the ground excitation pulse period $T_{\text{p}} = 0.5$ s. The right plot of Figure 2 shows the acceleration of the base for an antisymmetric Ricker pulse ground excitation given by

$$\ddot{u}_{\text{g}}(t) = \frac{a_{\text{p}}}{\beta_{\text{R}}}\left(\frac{4\boldsymbol{\pi}^2 t^2}{3T_{\text{p}}^2} - 3\right)\frac{2\boldsymbol{\pi} t}{\sqrt{3}T_{\text{p}}} e^{-\frac{14\boldsymbol{\pi}^2 t^2}{2\ 3T_{\text{p}}^2}} \tag{22}$$

where β_{R} is set to 1.38 such that the above function has a maximum equal to a_{p}. The pulse parameters are $a_{\text{p}} = 0.5\,g$ and $T_{\text{p}} = 0.5$ s. Wavelet analysis of the base mat acceleration time history gives a dominant pulse period of 0.56 s, indicating a slight excitation period elongation for the isolated structure. Note that the shape of the base mat excitation changes significantly compared with the ground excitation: it looks more like a constant acceleration pulse (approximated as a Gabor wavelet in Figure 2), a potentially more demanding pulse than the Ricker pulse because of its larger power [30]. The base mat excitation also has higher frequency components that might excite higher modes of the isolated structure. Despite these observations, the causes for large displacement ductility demand in inelastic isolated structures remain difficult to determine.

6. DIMENSIONAL ANALYSIS OF THE RESPONSE OF BASE-ISOLATED STRUCTURES TO ANALYTICAL PULSE EXCITATION

The destructive potential of near-source ground motions motivated the development of various closed-form analytical pulse functions that approximate the principal kinematic characteristics of such motions. The early work by Veletsos *et al*. [32] was followed by contributions from Hall *et al*. [33], Makris [34], Makris and Chang [35], Alavi and Krawinkler [36], and more recently by Mavroeidis and Papageorgiou [37]. Some of the most widely used analytical pulses (Apostolou *et al*. 2007 [38], Gazetas *et al*. 2009 [39] among others) are the symmetric Ricker pulse given by equation (21) and the antisymmetric Ricker pulse given by equation (22) [25, 26].

The well-defined characteristics of the analytical pulses make possible to use dimensional analysis to study the response of inelastic seismically isolated structures. Equations (19)–(22) show that the maximum structural deformation of a base-isolated inelastic structure excited by an analytical pulse is a function of 11 arguments:

$$u_{s_{max}} = f_1\left(T_{\text{b}}\frac{Q}{m_{\text{s}}+m_{\text{b}}}, u_{y_{\text{b}}}, \xi_{\text{b}}, T_{\text{s}}, \alpha, u_{y_{\text{s}}}, \xi_{\text{s}}, \gamma_{\text{m}}, a_{\text{p}}, T_{\text{p}}\right) \tag{23}$$

DOI: 10.1002/eqe

The maximum structural deformation of the corresponding elastic base-isolated structure (one that has the same mass and fundamental vibration period but different strength) is a function of the following nine arguments:

$$u_{s_{max},elastic} = f_2\left(T_b \frac{Q}{m_s + m_b}, u_{y_b}, \xi_b, T_s, \xi_s, \gamma_m, a_p, T_p\right) \tag{24}$$

There is a one-to-one correspondence between the yield displacement of the inelastic base-isolated structure u_{ys} and the force reduction factor R_y used to design it. Hence, equations (23) and (24) show that the displacement ductility μ of the inelastic base-isolated structure is a function of the following 11 variables:

$$\mu = \frac{u_{s_{max}}}{u_{y_s}} = f\left(T_b \frac{Q}{m_s + m_b}, u_{y_b}, \xi_b, T_s, \alpha, R_y, \xi_s, \gamma_m, a_p, T_p\right) \tag{25}$$

The 12 terms of equation (25) involve only two reference dimensions: length [L] and time [T]. According to Buckingham's Π-theorem [40, 41], equation (25) can be rewritten involving only 12-2 = 10 dimensionless terms, with the vibration periods normalized by the pulse period T_p:

$$\mu = \varphi_1\left(\frac{T_b}{T_p}, \frac{Q}{(m_s + m_b)a_p}, \frac{u_{y_b}}{a_p {T_p}^2}, \xi_b, \frac{T_s}{T_p}, \alpha, R_y, \xi_s, \gamma_m\right) \tag{26}$$

Alternatively, the structure vibration period T_s can be normalized using the isolation period T_b, and equation (25) can be written as

$$\mu = \hat{\varphi}_1\left(\frac{T_b}{T_p}, \frac{Q}{(m_s + m_b)a_p}, \frac{u_{y_b}}{a_p {T_p}^2}, \xi_b, \frac{T_s}{T_b}, \alpha, R_y, \xi_s, \gamma_m\right) \tag{27}$$

In this study, we assumed that the bearing yield displacement u_{yb} is very small ($u_{yb} \approx 0.25$ mm), such that the bilinear inelastic Bouc–Wen model corresponds to a spherical sliding bearing. Past studies (Makris and Chang [35], and Makris and Vassiliou [42]) have demonstrated that the response of isolated structures is indifferent to the exact value of the bearing yield displacement, making the results obtained in this study valid for isolation systems that use lead–rubber bearings, with larger values of u_{yb}, as long as they have the same hardening slope $\alpha_b k_b$ and the same strength Q. More important, according to [35] and [42], $\frac{u_{yb}}{a_p T_p^2}$ drops out of the equations (26) and (27), which then become

$$\mu = \varphi_2\left(\frac{T_b}{T_p}, \frac{Q}{(m_s + m_b)a_p}, \xi_b \frac{T_s}{T_p}, \alpha, R_y, \xi_s, \gamma_m\right) \tag{28}$$

$$\mu = \hat{\varphi}_2\left(\frac{T_b}{T_p}, \frac{Q}{(m_s + m_b)a_p}, \xi_b, \frac{T_s}{T_b}\alpha, R_y, \xi_s, \gamma_m\right) \tag{29}$$

The ratio of the maximum displacement of the inelastic system to the maximum displacement of the elastic system is defined as

$$\gamma = \frac{u_{s_{max}}}{u_{s_{elastic}}} = \frac{\mu}{R_y} = \varphi\left(\frac{T_b}{T_p}, \frac{Q}{(m_s + m_s)a_p}, \xi_b, \frac{T_s}{T_p}, \alpha, R_y, \xi_s, \gamma_m\right) \tag{30}$$

$$\gamma = \frac{u_{s_{max}}}{u_{s_{elastic}}} = \frac{\mu}{R_y} = \hat{\varphi}\left(\frac{T_b}{T_p}, \frac{Q}{(m_s + m_b)a_p}, \xi_b, \frac{T_s}{T_b}\alpha, R_y, \xi_s, \gamma_m\right) \tag{31}$$

A comparison of the maximum displacement ratio spectra plotted using T_s/T_p (equation (30)—Figure 4) and T_s/T_b (equation (31)—Figure 5) as dimensionless variables shows that normalizing

DOI: 10.1002/eqe

using the pulse period T_p results in a more consistent representation of the (relatively small) effect of the isolation period T_b. Henceforth, the time dimension will be normalized using the pulse period, and the results of dimensional analysis will be presented using the maximum displacement ratio spectra (plot of $\gamma = \mu/R_y$ versus structure–pulse period ratio T_s/T_p). The range of the abscissa was selected to cover the mathematically possible range of structure/pulse period ratios. Stiff structures can have natural periods as short as $T_s = 0.20$ s (Huang and Whittaker [43]), whereas energetic pulses from near source records can have periods as long as 3 s [42]. Hence, a practical lower bound for T_s/T_p can be set at 0.07.

6.1. *Principal findings*

Maximum displacement ratio spectra for an isolated structure with $\alpha_s = 0.02$, structural viscous damping $\xi_s = 0.02$, mass ratio $\gamma_m = 0.8$, bearing coefficient of friction $\mu_f = 0.05$, non-dimensional strength $\frac{Q}{(m_s+m_b)a_p} = \frac{\mu_f g}{a_p} = 0.05$, and no isolation system damping $\xi_b = 0$ are plotted in Figure 4 in natural coordinates for two values of R_y (1.5 and 3) and three values of the T_b/T_p ratio ranging from 2 to 4. The top plot is for a symmetric Ricker excitation, whereas the bottom plot is for an antisymmetric Ricker excitation. In the following discussion, the term 'counterparts' refers to the fixed-base and base-isolated structures that have the same strength reduction factor R_y.

From the data in Figure 4, it is evident that the displacement amplification ratio γ grows rapidly as the structure/pulse period ratio T_s/T_p becomes smaller. For small values of T_s/T_p (corresponding to

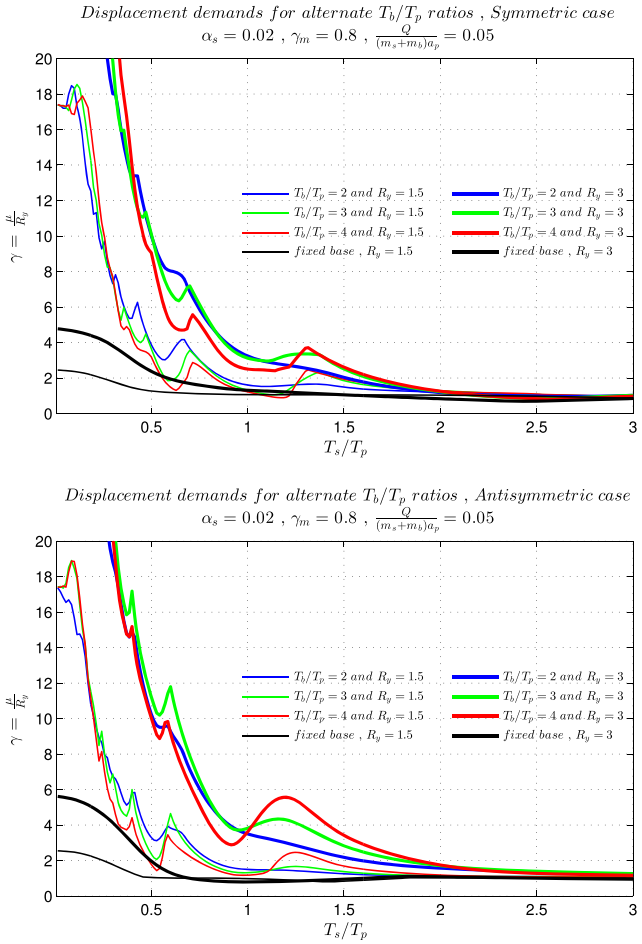

Figure 4. γ-T_s/T_p spectra for different values of normalized isolation periods T_b/T_p and force reduction factors R_y. Hardening $\alpha = 0.02$, mass ratio $\gamma_m = 0.8$ (heavy building), and normalized bearing yield force $\mu_f g/a_p = 0.05$. Top plot, symmetric Ricker pulse; bottom plot, antisymmetric Ricker pulse.

DOI: 10.1002/eqe

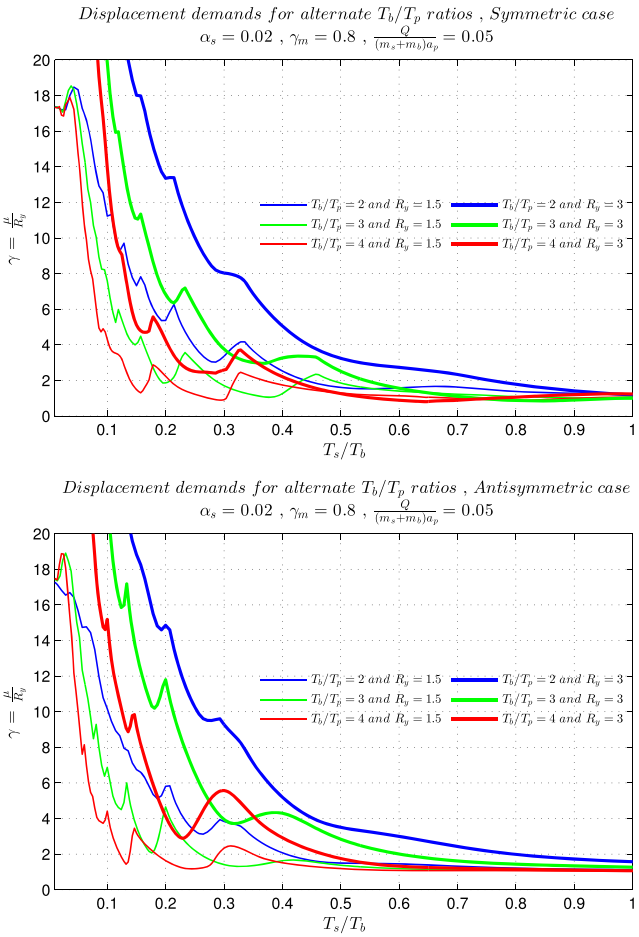

Figure 5. γ-T_s/T_b spectra for different values of normalized isolation periods T_b/T_p and force reduction factors R_y. Hardening $\alpha = 0.02$, mass ratio $\gamma_m = 0.8$ (heavy building), and normalized bearing yield force $\mu_f g/a_p = 0.05$. Top plot, symmetric Ricker pulse; bottom plot, antisymmetric Ricker pulse.

stiffer structures, the likely candidates for seismic isolation), the rate of growth of γ is much higher for base-isolated structures than it is for their fixed-base counterparts. For example, a structure with a force reduction factor $R_y = 3$ and a fundamental vibration period $T_s = 0.5$ s (giving $T_s/T_p = 1$) base isolated using spherical sliding bearings with $T_b = 2$ s (giving $T_b/T_p = 4$) and coefficient of friction $\mu_f = 0.025$, excited by a pulse with $T_p = 0.5$ s and $a_p = 0.5\,g$ would experience a displacement ductility demand of about 8, whereas its fixed-base counterpart would develop a displacement ductility demand of approximately 3.75. If the same seismically isolated structure is designed with an $R_y = 1.5$ (the value specified by the Eurocode and IBC for typical reinforce concrete frame structures), the displacement ductility demand induced by the Ricker pulse excitation would be about 3. Similar displacement amplification has been observed by Kikuchi *et al.* [17] for harmonic excitation, and Politopoulos and Pham [44] for earthquake excitation.

The 'counterpart' base-isolated and fixed-base structures have the same strength reduction factor, not the same strength. The base-isolated structure, therefore, has smaller yield strength than its fixed-base counterpart. Fixed-base structures designed to be very stiff are often very strong (Priestley *et al.* [45]), requiring very intense ground excitations to yield. On the contrary, base-isolated structures are designed only to remain essentially elastic for the base shear force transmitted by the base isolation system. If such structures are stiff relative to the duration of the excitation pulse, and if their strength reduction factor is overestimated (either because of an overestimate of yield strength or because of an underestimate of seismic force demand), the ductility demand they develop may be much larger than that expected according to the 'equal displacement' rule. Such

DOI: 10.1002/eqe

ductility demand may easily exceed the displacement ductility capacity of such stiff isolated structures and serve as a precursor to collapse. This observation leads to a conclusion that stiff base-isolated structures may not be ductile but quasi-brittle.

The data in Figure 4 provide guidance of the critical relative stiffness of base-isolated structures. We will assume that structures designed to respond inelastically can sustain the ductility demands in accordance with the 'equal displacement' rule, that is, $R_y = \mu$, or $\gamma = 1$. Using the data in Figure 4, the 'equal-displacement' region of the spectrum for inelastic fixed-base structures starts, roughly, when $T_s/T_p > 1$ for the symmetric Ricker pulse and when $T_s/T_p > 0.5$ for the antisymmetric Ricker pulse. In comparison, the 'equal-displacement' region of the spectrum for all inelastic base-isolated structures starts when $T_s/T_p > 2.5$ for both symmetric and antisymmetric Ricker pulses. This observation indicates that there is an effective shortening of the displacement-controlled region and a corresponding lengthening of the acceleration-controlled and velocity-controlled regions, of the response spectra for seismically isolated structures.

The data in Figure 4 also indicate that, for the considered values of the isolation period to excitation pulse ratio T_b/T_p equal to 2, 3, and 4, T_b/T_p is of minor importance for the displacement amplification factor γ, especially for small values of R_y. This observation does not hold for values of T_b/T_p smaller than 2, that is, for base-isolated structures whose isolation period is close to the predominant period of the excitation.

Combined, these three observations provide important design guidance for seismically isolated structures. Namely, typical short-period and medium-period seismically isolated structures should

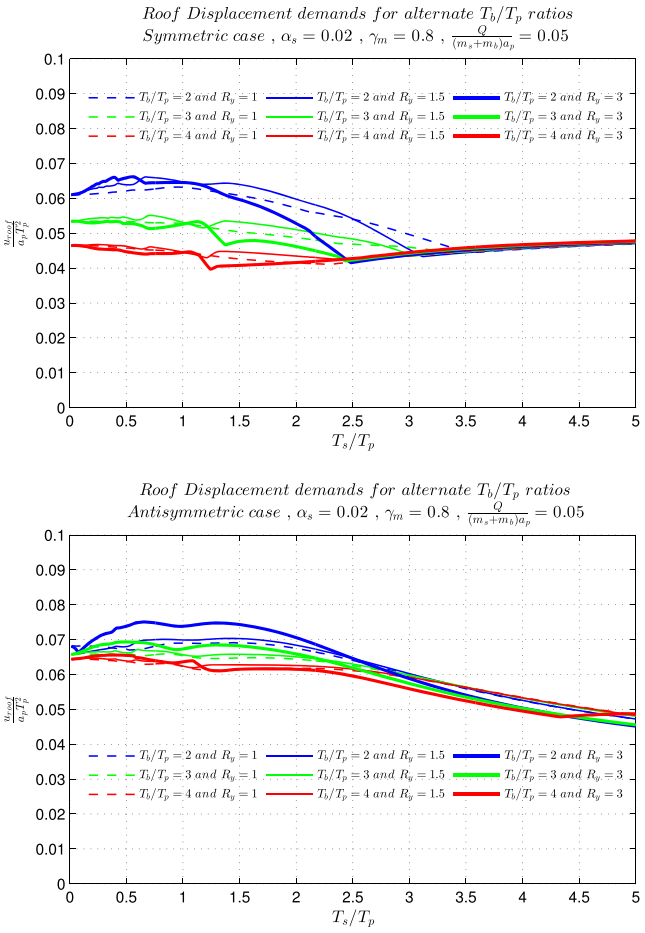

Figure 6. Structure displacement normalized with $a_p T_p^2$ plotted for different values of isolation periods (T_b/T_p) and different values of force reduction factor R_y. Top plot, symmetric Ricker pulse; bottom plot, antisymmetric Ricker pulse.

DOI: 10.1002/eqe

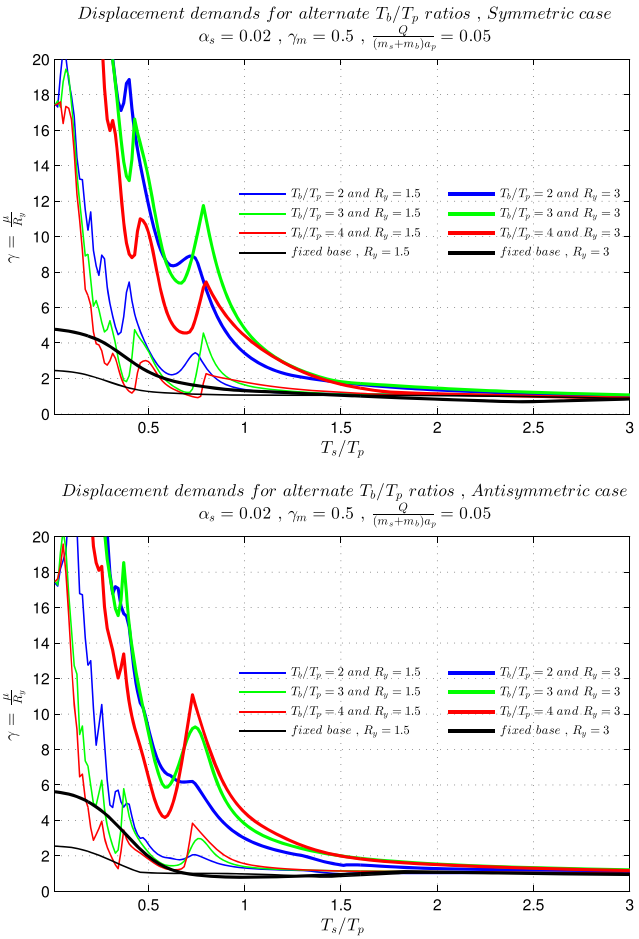

Figure 7. γ-T_s/T_p spectra for different values of normalized isolation periods T_b/T_p and force reduction factors R_y. Hardening $\alpha = 0.02$, mass ratio $\gamma_m = 0.5$ (light building), and normalized bearing yield force $\mu_f g/a_p = 0.05$. Top plot, symmetric Ricker pulse; bottom plot, antisymmetric Ricker pulse.

continue to be designed to remain elastic, with the force reduction factors accounting only for the possible overstrength of the isolated structures. Only the flexible, long-period isolated structures can be designed to respond inelastically following the conventional 'equal displacement' rule. Such structures are not typical candidates for seismic isolation: nevertheless, tall buildings have been seismically isolated in Japan [46] and in the USA [47, 48] and have performed well during the 2011 Great Tohoku Earthquake [14].

The maximum total (relative to the ground) roof displacements, u_{roof}, normalized using $a_p T_p^2$, for the structure–isolation systems in Figure 4 are plotted in Figure 6. It is worth noting that these maximum total displacement spectra are roughly the same in the elastic ($R_y = 1$) and the two inelastic cases ($R_y = 1.5$ and $R_y = 3$) across the range of different isolation periods (T_b/T_p). This observation leads to the conclusion that the maximum total roof displacement of the structure-isolation system with respect to the ground is preserved across the structure period spectrum (normalized with respect to the excitation pulse period). As Kikuchi *et al.* [17], Thiravechyan *et al.* [18], and Makris and Kampas [27] have shown, the vibration period that governs the response of the structure–isolation system is close to (and slightly smaller than) the isolation period T_b. Because the isolation period is relatively long, the structure–isolation system is in the displacement-controlled range of the pulse excitation response spectrum. Hence, the maximum total roof displacements change slightly with the variation of the seismic force reduction factor R_y for the isolated structure and can be predicted using the 'equal displacement' rule. However, the distribution of the total roof displacement between the base isolation system and the isolated structure changes depending on how the isolated structure responds. As shown in Figure 3, practically, all of the roof displacement

DOI: 10.1002/eqe

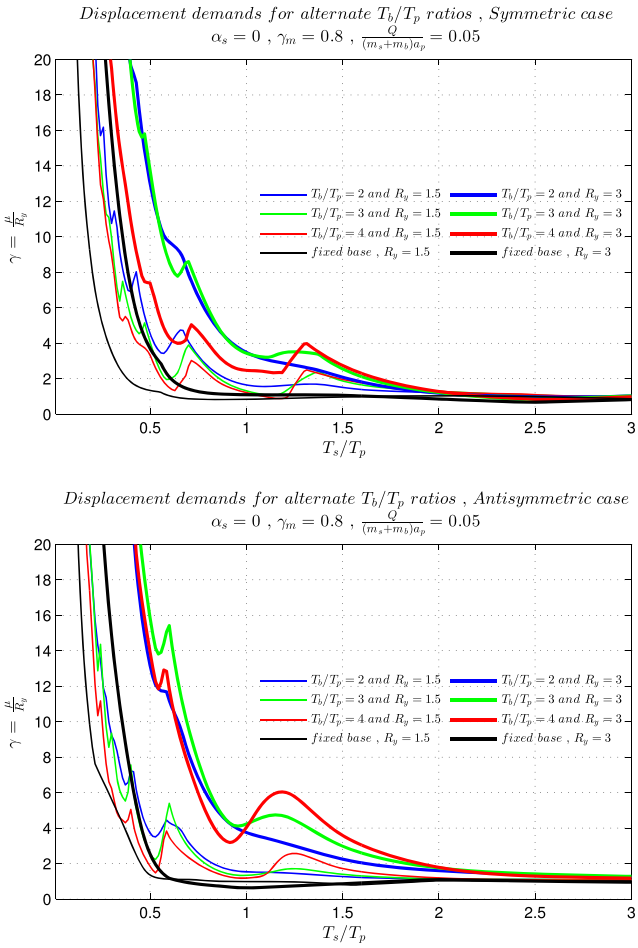

Figure 8. γ-T_s/T_p spectra for different values of normalized isolation periods T_b/T_p and force reduction factors R_y. Hardening $\alpha = 0.00$, mass ratio $\gamma_m = 0.8$ (heavy building), and normalized bearing yield force $\mu_f g/a_p = 0.05$. Top plot, symmetric Ricker pulse; bottom plot, antisymmetric Ricker pulse.

of the elastic isolated structure is accommodated by the bearings (the structural deformation is very small). In contrast, the total displacement of inelastic isolated structures is distributed between the structure and the isolation system. Furthermore, the distribution ratio is not constant but varies through the response time history depending on the sequence and duration of yielding events in the structure and the isolation system. More research is needed to fully understand why the inelastic deformation of typical base-isolated structures is larger than expected following the 'equal displacement' rule.

6.2. *Effects of design parameters*

The effects of the design parameters listed in equation (30) on the inelastic response of seismically isolated structures are investigated in this section. The effect of the weight of the seismically isolated structure is examined first. The γ-T_s/T_p spectra for a small value of the mass ratio, $\gamma_m = 0.5$, are plotted in Figure 7. This γ_m value corresponds to a one-story structure where the roof and the floor slab have the same mass. Compared with the case of a heavier structure (Figure 4), the lighter seismically isolated structure develops slightly smaller displacement ductility demands for the period ratio of interest for typical seismically isolated structures ($T_s/T_p < 1.5$) and for modest strength reduction factor values ($R_y = 1.5$). Hence, weaker interaction between the lighter structure and the seismic isolation system decreases the displacement ductility demands for the structure.

DOI: 10.1002/eqe

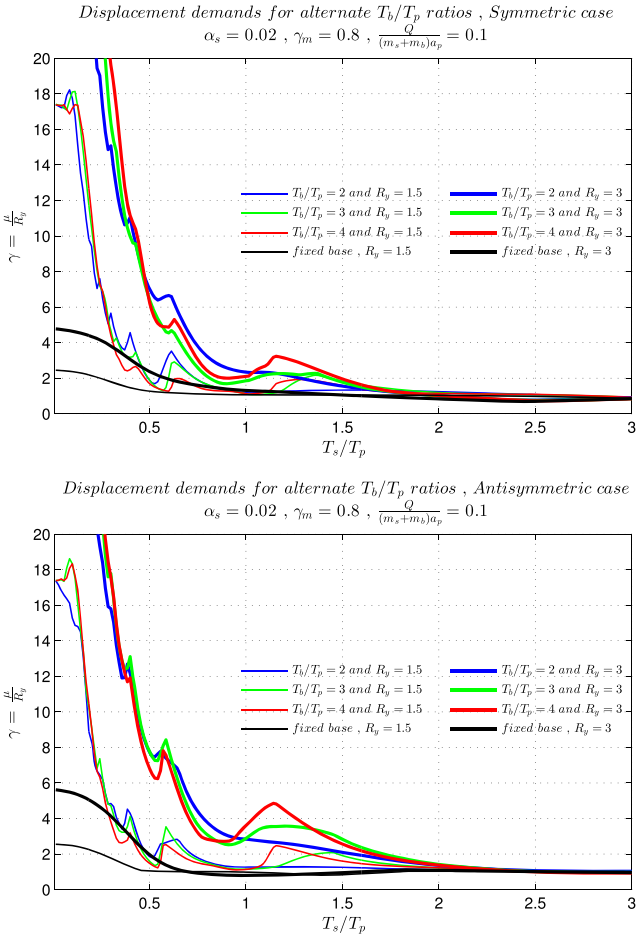

Figure 9. γ-T_s/T_p spectra for different values of normalized isolation periods T_b/T_p and force reduction factors R_y. Hardening $\alpha = 0.02$, mass ratio $\gamma_m = 0.8$ (heavy building), normalized bearing yield force $\mu_f g/a_p = 0.10$. Top plot, symmetric Ricker pulse; bottom plot, antisymmetric Ricker pulse.

The influence of structure stiffness hardening ratio, α_s, is investigated next in Figure 8, where the γ-T_s/T_p spectra are plotted for elastic perfectly plastic seismically isolated structures (hardening ratio $\alpha = 0$). As expected, post-yield hardening ($\alpha = 0.02$ in Figure 4) limits the magnitude of displacement of any structure, including seismically isolated ones. However, significant differences between the perfectly plastic and the hardening structures are apparent only when $T_s/T_p < 0.5$, that is, for stiff seismically isolated structures. This observation suggests that it is desirable to ensure that seismically isolated structures develop significant and sustainable hardening after they yield.

The effects of the seismic isolation system design parameters are investigated next. The influence of the normalized yield strength of the seismic isolation system (the bearings), $\frac{Q}{(m_s+m_b)a_p}$, is shown in Figure 9, where the γ-T_s/T_p spectra are plotted for twice-as-large value of $\frac{Q}{(m_s+m_b)a_p} = 0.1$ than those in Figure 4 where $\frac{Q}{(m_s+m_b)a_p} = 0.05$. Stronger bearings (larger Q) or a smaller excitation pulse (smaller a_p) slightly decreases the displacement ductility demand for the isolated structure. Note that when $\frac{Q}{(m_s+m_b)a_p}$ increases, the strength of the structure also changes so that R_y stays constant.

The γ-T_s/T_p spectra for a seismic isolation system with additional viscous dampers are shown in Figure 10. Evidently, the presence of the extra damping makes all of the spectra smoother, slightly elongates the displacement-controlled spectral region, reduces the importance of the pulse shape and the isolation period, but does not significantly reduce the displacement ductility demand on the inelastic seismically isolated structure.

DOI: 10.1002/eqe

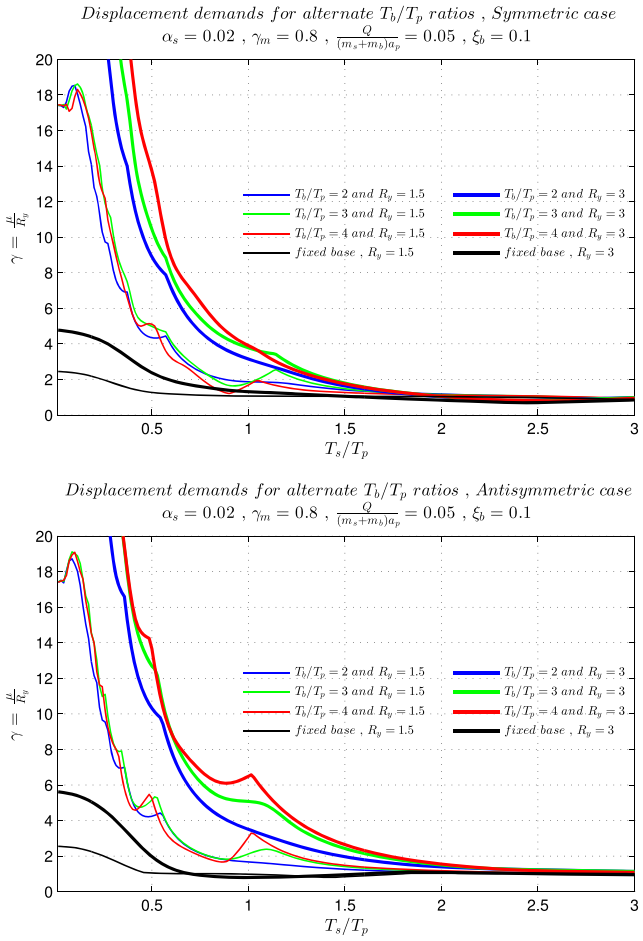

Figure 10. γ-T_s/T_p spectra for different values of normalized isolation periods T_b/T_p and force reduction factors R_y. Hardening $\alpha = 0.02$, mass ratio $\gamma_m = 0.8$ (heavy building), normalized bearing yield force $\mu_f g/a_p = 0.05$, and extra viscous damping at the base with $\xi_b = 0.1$. Top plot, symmetric Ricker pulse; bottom plot, antisymmetric Ricker pulse.

7. CONCLUSIONS

In this paper, we addressed the dynamics of inelastic seismically isolated structures. We used an inelastic 2-degree-of-freedom model to examine the dynamic response of such structures under analytical acceleration pulse ground excitation, and we organized the results by using dimensional analysis. The focus of our investigation was the relation between the yield strength of the isolated structure, its corresponding displacement ductility demand, and its fundamental vibration period. We find the following:

(1) The displacement ductility demand for a relatively stiff seismically isolated structure designed to yield under the expected seismic base shear grows rapidly with decreasing yield strength (for the same period) and increasing stiffness (for the same yield strength). We observe that a slight overestimate of the strength reduction factor may cause a disproportionately large displacement ductility demand that may exceed the ductility capacity of the seismically isolated structure and may lead to collapse. In this sense, the stiff inelastic seismically isolated structures are quasi-brittle.

(1) The spectral region where the seismically isolated structures are susceptible to such quasi-brittle behavior is significantly longer than that for the corresponding fixed-base structures. We

DOI: 10.1002/eqe

observe an effective shortening of the displacement-controlled region (where the 'equal displacement' rule applies) of the response spectrum for inelastic seismically isolated structures.

(2) Although the maximum displacement of the inelastic seismically isolated structure with respect to the ground is preserved, the distribution of this displacement between the seismic isolation system and the structure varies considerably and depends on the sequence and duration of the yielding events in the structure and the isolation system.

(3) It is desirable that inelastic seismically isolated structures develop significant and sustainable post-yield hardening to limit the magnitude of displacement and thus control the ductility demand.

(4) Stronger seismic isolation bearings and additional damping in the seismic isolation system reduce the displacement ductility demand for the seismically isolated structures. The choice of the seismic isolation period does not have a significant effect on the relationship between the strength reduction factor (R_y), the ductility (μ), and the structural period (T_s) as long as the isolation period is at least twice as long as the period of the pulse excitation.

On the basis of the aforementioned findings, we conclude that designing typical seismically isolated structures to behave elastically, as prescribed by current seismic design codes, is not overly conservative but a necessity that emerges from the fundamental dynamics of such structures. The advantages of correctly designed seismically isolated structures over their fixed-based counterparts are (i) high confidence in achieving the target seismic performance objectives; and (ii) control of the life-cycle costs of the structure. These advantages should be evaluated against the increased initial investment in the seismic isolation system to determine the seismic design strategy that best suits the economic needs and capabilities of the investors and owners of the structure.

REFERENCES

1. Structural Engineering Institute. Minimum design loads for buildings and other structures (Vol. 7, No. 5). Amer Society of Civil Engineers, 2010.
2. CEN, Eurocode 8: design of structures for earthquake Resistance—Part 1: general rules, seismic actions and rules for buildings. EN 1998–1:2004. Comité Européen de Normalisation, Brussels, 2004.
3. Newmark NM, Hall WJ. Seismic design criteria for nuclear reactor facilities, *Report 46*, Building Practices for Disaster Mitigation, National Bureau of Standards, 1973; 209–236.
4. Veletsos AS, Newmark NM. Effect of inelastic behaviour on the response of simple systems to earthquake motions. *Proceedings of the 2nd World Conference on Earthquake Engineering*, Tokyo, Japan, 1960; 895–912.
5. Veletsos AS, Newmark NM, Chepalati CV. Deformation spectra for elastic and elastoplastic systems subjected to ground shock and earthquake motion. *Proceedings of the 3rd World Conference on Earthquake Engineering*, New Zealand, vol. **II**, 1965; 663–682.
6. Elghadamsi FE, Mohraz B, Inelastic earthquake spectra. *Earthquake Engineering Structural Dynamic* 1987; **15**:91–104.
7. Riddell R, Hidalgo PA, Cruz EF. Response modification factors for earthquake resistant design of short period buildings. *Earthquake Spectra* 1989; **5**(3):571–590.
8. Nassar AA, Krawinkler H. Seismic demands for SDOF and MDOF systems. *Report No. 95, The John A.Blume Earthquake Engineering Center*, Stanford University, Stanford, 1991.
9. Vidic T, Fajfar P, Fischinger M. Consistent inelastic design spectra: strength and displacement. *Earthquake Engineering Structural Dynamic* 1994; **23**:502–521.
10. Miranda E, Bertero VV. Evaluation of strength reduction factors for earthquake-resistant design. *Earthquake Spectra* 1994; **10**:357–379.
11. Miranda E, Ruiz-García, J. Evaluation of approximate methods to estimate maximum inelastic displacement demands. *Earthquake Engineering Structural Dynamic* 2002; **31**:539–560.
12. Kelly JM. *Earthquake-Resistant Design with Rubber*. Springer: London, 1997.
13. Japanese Ministry of Land, Infrastructure and Transport, Notification No. 2009–2000, Technical Standard for Structural Specifications and Calculation of Seismically Isolated Buildings. (in Japanese). 2000.
14. Takayama M, Morita K, Seismic response analysis of seismically isolated buildings using observed records due to 2011 Tohoku earthquake, *Proceedings of the 15th World Conference on Earthquake Engineering*, Lisboa, Portugal, 2012.
15. Constantinou MC, Quarshie JK. Response modification factors for seismically isolated bridges. *Report No. MCEER-98-0014*, Buffalo, NY, 1998.
16. Ordonez D, Foti D, Bozzo L. Comparative study of the inelastic response of base isolated buildings. *Earthquake Engineering Structural Dynamic* 2003; **32**:151–164.
17. Kikuchi M, Black CJ, Aiken ID. On the response of yielding seismically isolated structures. *Earthquake Engineering and Structural Dynamics* 2008; **37**(5):659–679.

DOI: 10.1002/eqe

18. Thiravechyan P, Kasai K, Morgan TA. The effects of superstructural yielding on the seismic response of base isolated structures. Joint Conference proceedings, 9th International Conference on Urban Earthquake Engineering / 4th Asia Conference on Earthquake Engineering, Tokyo, Japan, 2012; 1451–1458.
19. Kelly, JM. Seismic isolation. *Earthquake Engineering, from Engineering Seismology to Performance-Based Engineering*, Bozorgnia Y, Bertero VV (Eds.). CRC Press: Boca Raton, FL, 2004.
20. Chopra AK. *Dynamics of Structures: Theory and Applications to Earthquake Engineering*. Prentice-Hall: Englewood Cliffs, NJ, 1995.
21. Miranda E. Evaluation of site-dependent inelastic seismic design spectra. *Journal of Structural Engineering (ASCE)* 1993; **119**(5):1319–1338.
22. Ruiz-García, J, Miranda, E. Inelastic displacement ratios for evaluation of structures built on soft soil sites. *Earthquake Engineering and Structural Dynamics* 2006; **35**:679–694.
23. Wen YK. Approximate method for nonlinear random vibration. *Journal of the Engineering Mechanics Division* 1975; **101**(4):389–401.
24. Wen YK. Method for random vibration of hysteretic systems. *Journal of the Engineering Mechanics Division* 1976; **102**(2):249–263.
25. Ricker N. Further developments in the wavelet theory of seismogram structure. *Bulletin of the Seismological Society of America* 1943; **33**:197–228.
26. Ricker N. Wavelet functions and their polynomials. *Geophysics* 1944; **9**:314–323.
27. Makris N, Kampas G. The engineering merit of the "effective period" of bilinear isolation systems, *Earthquakes and Structures* 2013; **4**(4):397–428, (in press).
28. Makris N, Black CJ. Dimensional analysis of rigid-plastic and elastoplastic structures under pulse-type excitations. *Journal of Engineering Mechanics (ASCE)* 2004; **130**(9):1006–1018.
29. Makris N, \ CJ. Dimensional analysis of bilinear oscillators under pulse-type excitations. *Journal of Engineering Mechanics (ASCE)* 2004; **130**(9):1019–1031.
30. Vassiliou MF, Makris N. Analysis of the rocking response of rigid blocks standing free on a seismically isolated base. *Earthquake Engineering and Structural Dynamics* 2011; **41**(2):177–196.
31. Vassiliou MF, Makris N. Estimating time scales and length scales in pulse-like earthquake acceleration records with wavelet analysis. *Bulletin of the Seismological Society of America* 2011; **101**(2):596–618.
32. Veletsos AS, Newmark NM, Chelepati CV. Deformation spectra for elastic and elastoplastic systems subjected to ground shock and earthquake motions. *Proceedings of the 3rd World Conference on Earthquake Engineering*, vol. II, Wellington, New Zealand, 1965; 663–682.
33. Hall JF, Heaton TH, Halling MW, Wald DJ. Near-source ground motion and its effects on flexible buildings. *Earthquake Spectra* 1995; **11**(4):569–605.
34. Makris N. Rigidity–plasticity–viscosity: can electrorheological dampers protect base-isolated structures from near-source ground motions? *Earthquake Engineering and Structural Dynamics* 1997; **26**:571–591.
35. Makris N, Chang S-P. Effect of viscous, viscoplastic and friction damping on the response of seismic isolated structures. *Earthquake Engineering and Structural Dynamics* 2000; **29**(1):85–107.
36. Alavi B, Krawinkler H. Effects of near-source ground motions on frame-structures. *Technical Report No. 138*, The John A. Blume Earthquake Engineering Center, Stanford University, 2001.
37. Mavroeidis GP, Papageorgiou AS. A mathematical representation of near-fault ground motions. *Bulletin of the Seismological Society of America* 2003; **93**(3):1099–1131.
38. Apostolou M, Gazetas G, Garini E. Seismic response of slender rigid structures with foundation uplift. *Soil Dynamics and Earthquake Engineering* 2007; **27**:642–654.
39. Gazetas G, Garini E, Anastasopoulos I. Effect of near-fault ground shaking on sliding systems. *Journal of Geotechnical Engineering, ASCE*, **135**(12):1906–1921, 2009.
40. Buckingham, E. On physically similar systems; illustrations of the use of dimensional equations. *Physical Review* 1914; **4**(4):345–376.
41. Barenblatt GI. *Scaling, Self-Similarity, and Intermediate Asymptotics*. Cambridge University Press: Cambridge, U.K., 1996.
42. Makris N, Vassiliou MF. The existence of "complete similarities" in the response of seismic isolated structures subjected to pulse-like ground motions and their implications in analysis. *Earthquake Engineering and Structural Dynamics* 2011; **40**:1103–1121.
43. Huang, YN, Whittaker, AS. Performance assessment of conventional and base-isolated nuclear power plants for earthquake and blast loadings, *Technical Report MCEER-08-0019*, State University of New York at Buffalo, Buffalo, NY, 2008.
44. Politopoulos, I, Pham HK. Sensitivity of seismically isolated structures. *Earthquake Engineering and Structural Dynamics* 2009; **38**(8):989–1007.
45. Priestley, MJN, Calvi GM, Kowalsky MJ. *Direct displacement-based seismic design of structures*. IUSS Press: Pavia, Italy, 2007.
46. Kani N. Current state of seismic-isolation design, *Journal of Disaster Research* 2009; **4**(4):175–181.
47. Youssef N, Nuttall B, Hata O, Tahtakran O, Hart, GC. Los Angeles City Hall. *Structural Design of Tall Buildings* 2000; **9**:3–24.
48. Youssef, N. Viscous dampers at multiple levels for the historic preservation of Los Angeles City Hall. *Structural Design of Tall Buildings* 2001; **10**:339–350.

DOI: 10.1002/eqe